Guidelines for the design of tyre sensor housings

Int J Adv Manuf Technol manuscript No.
(will be inserted by the editor)

Guidelines for designing tyre sensor housings

Francesco Di Monaco · Sandro Moos · Stefano Tornincasa · Enrico Vezzetti

Received: date / Accepted: date

Abstract The next generation of tyre sensors are bonded directly to the inner-liner with the purpose of measuring important parameters like strain, tyre forces, contact pressure, tyre-road friction coefficient, tyre wearout or vehicle load. These measures can be used by the car control unit to improve the active or passive safety of the vehicle.

Because all these sensor packages are bonded and kept into position by specifically designed rubber-housings, they become safety critical components.

In this work it is presented a method to set-up a computationally light-weight FEM simulation, in order to recreate the working conditions the rubber-housings and the sensor node are subjected. The proposed methodology has been developed for the Pirelli Cyber™ Tyre project.

The method considers as input data the tyre deformed shape and the inertial forces acting on the sensor node, then it impose them to a simplified model of the tyre and to the sensor node, by means of user-defined routines executed by the FEM solutor. As a result, it is possible to estimate the stress distribution inside the components, with the aim of optimizing their shape, sizes and mass, so to guarantee the mechanical resistance of the designed housing to the severe conditions of the tyre environment. The resulting optimised shape also allows the reduction of the costs for building prototyping molds of the rubber-housing components.

By providing a reliable support for the tyre sensors, this methods contributes to strenghten the road safety.

Keywords Tyre sensor · FEM · Rubber house

Francesco Di Monaco · Sandro Moos · Stefano Tornincasa · Enrico Vezzetti
Politecnico di Torino – Department of Management and Production Engineering (DIGEP).
Tel.: +39-011-0907294
Fax: +39-011-0907299
E-mail: sandro.moos@polito.it

1 Introduction

Tyres are a key characteristic in ensuring the vehicle safety and efficiency. The world wide legislation defines strict parameters for their production and also requires their monitoring in order to ensure the proper functional conditions.

The TREAD Act approved in the 106th Congress (1999 - 2000, H.R.5164) [21] made the United States Department Of Transportation (NHTSA) to release the FMVSS No. 138 [22], which requires the installation of a Tyre Pressure Monitoring System (TPMS) in new passenger cars, MPVs., trucks, and buses that have a gross vehicle weight less than about 4,500 kg.

These devices use wheel modules containing wireless radio transmitters to pass the pressure and temperature data, across the rotating wheel-chassis boundary to the vehicle control unit as in Ergen et al. [8]. The objective is to give an in-car warning to the driver when a loss of pressure occurs in any tyre, in the interests of optimum fuel consumption and road safety.

With the regulation EC N. 661/2009 [24], the European Union required all new models of passenger cars to be equipped with a TPMS, starting from November 1st, 2012. Other countries, such as South Korea, Russia, Indonesia, the Philippines, Israel, Malaysia and Turkey defined similar rules.

After these laws were passed, many companies responded to the new market opportunity by developing new and more functional sensor units. Many sensor types are nowadays available, with different shape, weight, functionalities, ranging from simple monitors to more evolute sensors able to measure the tyre strain as in Matsuzaki et al. [19, 20], the estimation of slip angle, tyre forces, slip ratio, as in Erdogan et al. [6, 7] and tyre-road friction coefficient, road condition, tyre wearout, vehicle load as in Flatscher et al. [10]

The latest devices that extract the tyre parameters from acceleration measures made directly on the inner-liner (IL),

are usually packaged as compact sensor units as in Chee et al. [5] and in Audisio [1] and all of them have a common functional requirement: to be bonded securely inside the tyre.

Many of the works regarding devices for in-tyre energy production (harvester) or sensors, as in Roundy et al. [28, 27] and Bonisoli et al. [3], display a schematic rubber-housing (RH) connecting each device to the internal surface of the tyre.

Some indications regarding the RHs can be found in patents as in Koch et al. [16], which presents sensor shapes corresponding to a rounded prism completely enveloped by rubber and a cylinder half encased into rubber. The bottom bonding surface can be smooth or rough.

Martin et al. [18] defines a mounting device made of a rubber patch with a block protruing radially toward the wheel axis and forming a contour (for example a dovetail profile) on which is fitted the electronic package that includes a complementary channel.

Bertrand et al. [2] shows many patch layouts in which the sensor can be inserted and they differs for the shape of the bounding surface, while Hironaka [15] shows an electronic device bridging two rubber patches bounded to the IL.

Bonisoli et al. [4] described a cylindrical energy harvester, with an housing fixed on a crown portion of the tyre, that extends accordingly to a longitudinal axis. It contains an electrical winding and a magnet movable within the housing and winding. It is activated by the force variations that act on the device every time it passes at the footprint of the tyre.

In these patents, the shape of the RH is simply sketched, very few information are provided about the performances and employment conditions (speed, temperature, shock resistance ...) and the material is defined only in general terms.

The RHs, bonded directly to the IL of the tyre, are subjected to severe condition: during the wheel turn they and the carried sensor packages are subjected to the centifugal force; before and after the contact with the pavement they are subjected to the high deformation gradient of the tyre and to the corresponding high radial and tangential accelerations. A lateral acceleration, mainly due to the camber angle, altough smaller than the other components, is also present.

The RH must be able to bear the high forces due to the high accelerations the sensor package is subjected (at 200 km/h the acceleration magnitude at the IL is about $3000\,g$ [8]) and it must stand the deformation gradient imposed by the wheel deformation. According to [17] a maximum acceleration peak of $4000-5000\,g$ should be taken into account for in-tyre mounted devices in order to fulfill the lifetime and automotive quality requirement. For this reason the sensor package should be lightweight, robust and small.

The FEM modelling of tyres has been reviewed by Ghoreishy [12]: due to the extremely complex structure of tyres, different methods have been proposed to simulate the rolling tyre. If the applied load remains in the tyre vertical symmetry plane (normal to the revolution axis), 2D models can be used, otherwise it is nescessary to use 3D models. A full 3D model has the disadvantage of being extremely computationally expensive but, on the other hand, allows to simulate almost all the possible work conditions of the tyre.

In an accurate model of the tyre several nonlinearities have to be considered mainly regarding geometry, material and contact. In case of static simulation the typical material model used for tyre rubber is Mooney-Rivlin hyperelastic model, while for reinforcing fibers a linear elastic model is used. In case of dynamic simulation a viscoelastic model of the rubber is necessary to take into account the energy dissipation during the tyre rolling.

In [11] Ghoreishy presented an axisymmetric 2D model of the tyre and a full 3D model. The 2D model is suitable for the inflation analysis only, whereas the 3D model generated by revolving the 2D elements about the symmetry axis has been used for footprint and steady state rolling analysis. To improve the accuracy of computation the mesh is more refined in the contact zone. The same procedure is used to generate the 3D mesh by Yangjin et al. in [32], while rebar elements are used to simulate the reinforcing cord.

Considering the complexity of the tyre model the approach of simulating the rotation of a full 3D FEM model of the tyre, inserting into it the RH model with the sensor unit, is unsuitable and the resulting model will be computationally intensive to solve because it also presents a two scale problem: the tyre model, modelled as a composite structure of many layers, and a much smaller RH, requiring very small elements to obtain a proper description of the internal stress field.

Given the working conditions and loads here recalled, it is evident that the RH is also a safety critical component because it must provide a reliable support for the sensor, without breaking and releasing the sensor free into the tyre chamber. With a market of about 1.5 billions of tyres produced each year [14], much care must be given in dimensioning correctly the RH, by considering the sensor package shape and by optimizing the housing weight.

Unfortunately, there is no evidence in the literature of any FEM simulation that is able to guide the designer during the RH development. Hence, this paper proposes a method for the set-up of a FE simulation that considers the most important phenomena occuring during the tyre revolution and reduces the problem complexity. Prototypes built on the RH shape resulting from the analysis should be able to immediately pass the experimental tests, so reducing the prototipation costs.

2 Methodology

The aim is to reproduce the deformation states and the inertial effects acting on the RH and sensor node, in order to evaluate the stress state of the components and make the required adjustment to the geometry, so to guarantee the mechanical resistance of the assembly.

The characterizing phenomena will be managed in the simulation by means of user defined coding, implemented by means of some FEM subroutines the user is allowed to program directly. On the RH and the sensor they impose the deformation of the tyre when it passes on the contact surface (planar road, drum, curb ...) and the corresponding radial, tangential and lateral forces.

The points of the methodology will be described in detail in the following sections, then they will be integrated in an overall environment able to reproduce the significant phenomena of the tyre rolling. Some indications will be given about material, bonding, the organization and integration of the information required for the simulation.

The main assumptions are a steady state rolling, at a reference vehicle velocity V_0, the FEM use a simple static simulation and the cross curvature of the tyre is neglected. Here the tyre model has been simply approximated to the IL layer.

2.1 Imposed deformations on the inner-liner

Sources like Fervers [9] define an accurate 2D modelling of the tyre considering, threads, carcass cords, belt cords, rim and the air filled volume that is placed on many different kind of terrain (rigid road, curb climbing, soft soil and the corresponding friction coefficient) with different vertical loads, with and without the engine propelling action and at different air pressures. Hence it is possible to calculate the deformed shapes of the tyre in many different working conditions. The deformed shapes are usually measured in the symmetry plane of the tyre and can be expressed, as in figure 1, in terms of Cartesian or Polar coordinates as function of the angular position α.

For the use of this work, it has been considered the polar representation of the tyre deformed shape $R(\alpha)$ and it has been imposed as a displacement to the IL patch. The dimensionless $R_d(\alpha) = R(\alpha)/R_0$ parameter defines a particular deformed "shape" that depends on the working conditions of the tyre and can be more generally adapted to different tyre diameters. Usually the shape is known only at specific equally angularly spaced α_j, for a total of n finite number of positions.

Figure 2 defines the geometry considered in the simulation. The 2a sketch identifies the tyre centered in the origin and it also defines the position of the RH as symmetrycal to the X and Z planes, at a distance corresponding to the patch inner radius R_p, in the initial undeformed configuration. The

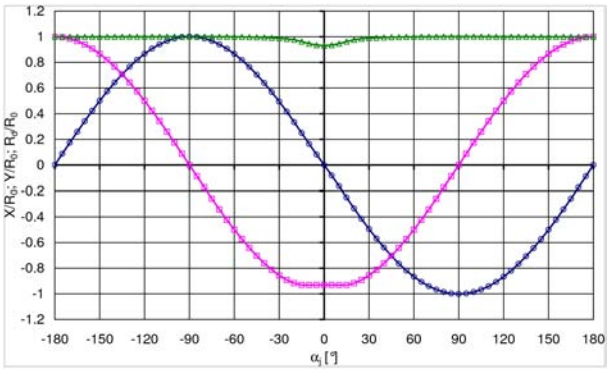

Fig. 1 Deformed contour of the tyre. The coordinates of the measured points are expressed in Cartesian and Polar systems and made dimensionless by dividing by R_0, the undeformed tyre radius. △ R_d/R_0; ◯ X/R_0; □ Y/R_0. The values are usually known at α_j discrete angular positions. (Numerical results from a 3D FEM model, courtesy of Pirelli Tyre S.p.A.)

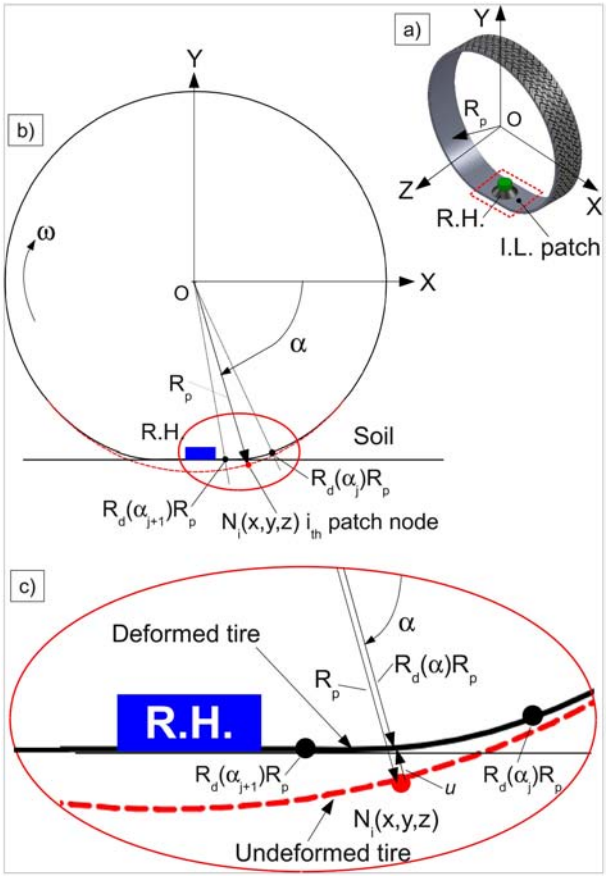

Fig. 2 Sketch of the FEM imposed deformations. a) reference axes, RH position, IL patch b) Node angular position c) displacement required to move the node from the undeformed to the deformed shape.

reference axes are also shown, with Z along the wheel axis. The geometry of the tyre is considered as a simple extrusion, without the cross-section curvature and later it will be limited to a resctricted patch in the FEM model to reduce the computational time.

The aim here is to define the formulation required for transforming the mesh nodes of the IL patch from the undeformed shape to the deformed one. In the 2b sketch the position of an i element node $N_i(x,y,z)$ on the IL patch is shown. Its angular position α in the undeformed shape R_p can be calculated from the coordinates as $\alpha = \arctan(y/x)$ and its radial position in the deformed configuration will be $R_d(\alpha)R_p$.

If the mesh node angular position is not coincident with one of the known α_j subdivision of the deformed tyre shape, it is necessary to provide an interpolated radius value between the nearest subdivisions. With α_j the nearest lower known angular position and α_{j+1} the nearest higher one, $\alpha_j \leq \alpha \leq \alpha_{j+1}$, the corresponding positions can be calculated as $R_d(\alpha_j)R_p$ and $R_d(\alpha_{(j+1)})R_p$ and the deformed radius $R_d(\alpha)$ at the α position can be defined by interpolation of those values:

$$R_d(\alpha) = R_d(\alpha_j) + \frac{\alpha - \alpha_j}{\alpha_{j+1} - \alpha_j}\left(R_d(\alpha_{j+1}) - R_d(\alpha_j)\right) \tag{1}$$

Then, the u displacement vector (figure 2c), at an α angular position, will be the difference of the undeformed radial position R_p and the deformed value $R_d(\alpha)R_p$; its projections on the (X,Y) reference axis will be:

$$u_x = R_p(R_d - 1)\cos(\alpha) \tag{2a}$$

$$u_y = R_p(R_d - 1)\sin(\alpha) \tag{2b}$$

In the FEM simulation it is defined a deformation step in which the IL model is changed from the undeformed to the deformed tyre shape. In this step the material is gradually deformed to avoid convergence problems. So the displacement defined by equations 2a and 2b will be imposed as a linear ramp during the step time t, with $t \in [0,1]$. Moreover it is defined an α_i parameter that is an initial angle offest for the tyre deformed shape, useful to start the simulation from a required value. With these considerations the equations 2a, 2b become:

$$u_x = R_p(R_d - 1)\cos(\alpha + \alpha_i)t \tag{3a}$$

$$u_y = R_p(R_d - 1)\sin(\alpha + \alpha_i)t \tag{3b}$$

In a following simulation step, it is required to simulate the rotation of the wheel, with the aim of subjecting the RH to all the deformed shapes the tyre undergo during the rotation. This is done by inserting into equations 3a and 3b the rotation angle α_r:

$$\alpha_r = \omega_0 t \tag{4}$$

where t is the simulation time and ω_0 the wheel angular speed, corresponding to the reference vehicle speed V_0. Then equations 3a and 3b will be implemented as follows:

$$u_x = R_p(R_d - 1)\cos(\alpha + \alpha_r + \alpha_i) \tag{5a}$$

$$u_y = R_p(R_d - 1)\sin(\alpha + \alpha_r + \alpha_i) \tag{5b}$$

where the argument of the trigonometric functions is the sum of the angular position of the node mesh α, the rotation angle α_r and the offset angle α_i: $\alpha_t = \alpha + \alpha_r + \alpha_i$.

The sum of the rotation angle α_r will cause α_t not always coincident with the α_j angles for which the deformed tyre shape R_d is known. When it assume intermediate values it is necessary define an interpolated values. First it is found the α_j angular position that precedes α_t as:

$$j = \texttt{MOD}\left(\texttt{INT}\left(\alpha_t \frac{n}{360}\right), n\right) + 1 \tag{6}$$

the `INT` function change the variable type from real to integer, so that is suited for addressing an array element, and rounds down the value to the largest integer that does not exceed its range. The `MOD` function computes the remainder of an integer division ($\texttt{MOD}(x,y) = x - \texttt{INT}(x/y)y$) of the angular position and it is used to make it periodic in the wheel rotation. The $+1$ is necessary to address properly the data array, because the routines will be implemented in Fortran [23], that starts numbering the vectors elements from 1 and not from 0. It is possible to use equation 1 to make the interpolation using α_t instead of the α angle.

To reduce the computational effort it is preferable to limit the simulation near the tyre/road contact patch, neglecting the angles where the tyre is rotating in the wheelarch and it is subjected only to the centrifugal force. The time for simulating a complete tyre revolution $t_{1R} \in [0, 2\pi/\omega_0]$, can be reduced using the offset angle α_i to make the simulation start with the deformed shapes near the RH and to stop the simulation after rotation reach an appropriate α_f angle.

The step time corresponding to a partial revolution that starts at α_i position and ends at α_f (figure 3a,e) can be calculated as:

$$t_s = \frac{\alpha_f - \alpha_i}{\omega_0} \tag{7}$$

with α_i and α_f apppropriately chosen by the analyst.

In the static simulation are inserted the step time of equation 7, the initial time increment and the maximum time increment allowed during the computation. Here it is chosen to set both time increment to a value corresponding to the discretization angle for which the deformed shape is known.

Figure 3 displays the model of a IL developed for 360°, in order to better show the effect of using the approach here defined.

In figure 3a the cylindrical model of the tyre has been deformed using the imposed displacement of equations 5a and 5b. Here it is shown the deformed shape positioned correspondingly to α_i angular position at the simulation step time $t = 0$. Figures 3b,c,d show other intermediate deformed shapes due to the increment of α_r with the step time and 3e shows the last position computed corresponding to α_f. The sensor node is always aligned below the origin.

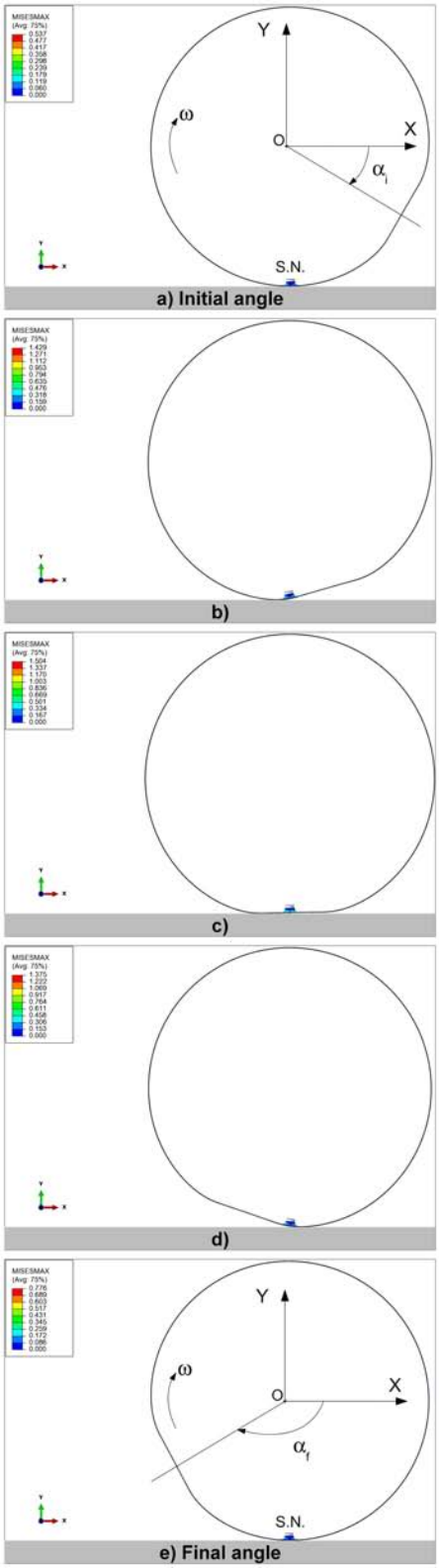

Fig. 3 Deformed shape positions. a) The circular wheel has been deformed with the contact patch shape in the initial position α_i. b, c, d) Other intermediate position of the deformed shape. e) Final simulation angle α_f. The sensor node position does not change in the FEM reference system. The deformations are rotated under it.

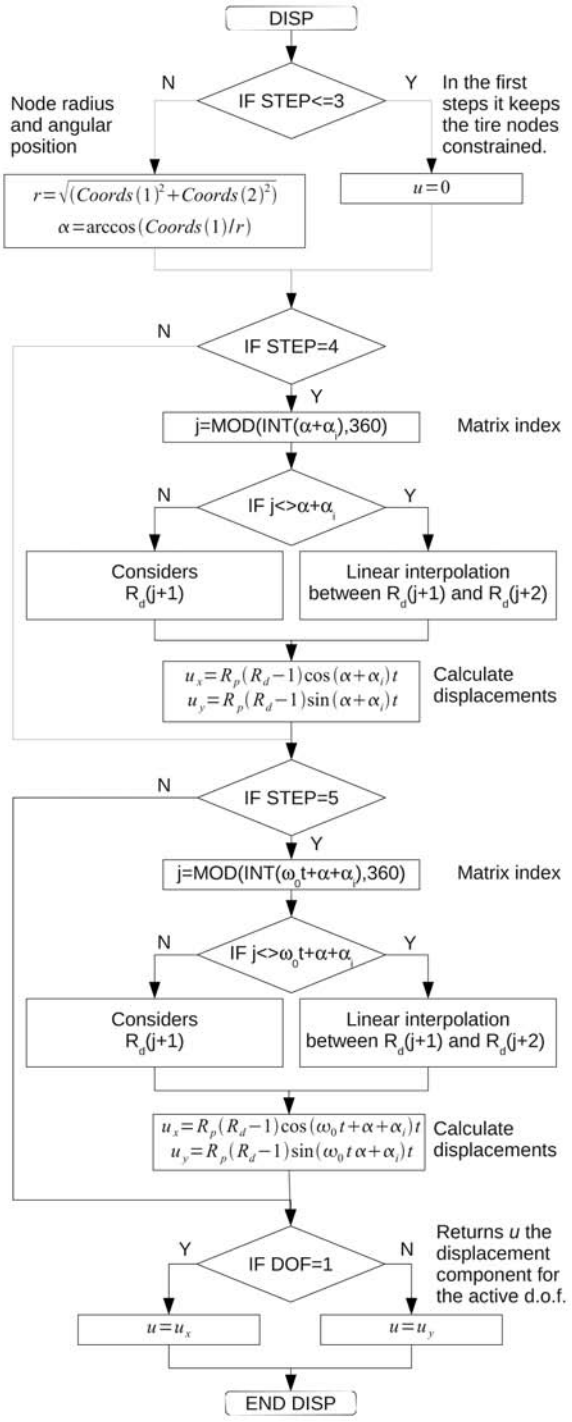

Fig. 4 Flow chart of the `DISP` routine.

Figure 4 shows the flow chart of the program implemented into the Abaqus/Standard `DISP` routine [31].

The approach is tought modular: the deformed shape is saved in a text file that is loaded in the FEM software by means of a suitable routine at the beginning of the simulation. After a small library of deformed shapes is built, it is

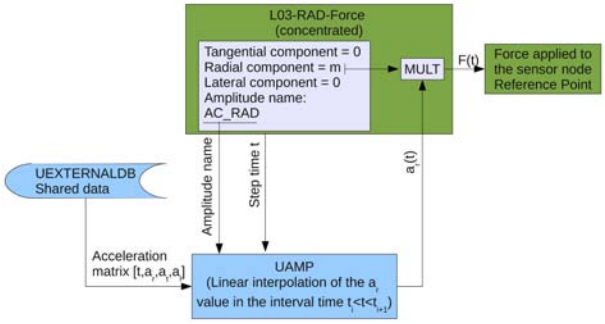

Fig. 5 Computation of the concentrated radial force, acting on the sensor node, by the specification of the components and a user defined amplitude. The component is the sensor mass m, the amplitude returns the acceleration $a_r(t)$ to which the material is subjected at the simulation time t.

possible to change from a simulation condition to another by simply a new file with the routines.

Concluding, this formulation allows to impose a displacement field to an IL patch that is continuously updated during the FEM computation in order to subject the bonded RH and sensor node to all the deformations the tyre undergo when contacting the ground, without making the nodes of the mesh rotating around the origin. Moreover, it is not necessary to implement a full 360° model for the tyre, but a patch covering an angular span wider than the RH base, so that the borders effect can be neglected, is sufficient. This will be further described in section 2.3.

2.2 Application of the inertial forces on the sensor node

A static simulation in itself can not replicate the effects of the centripetal acceleration and of the accelerations due to the tyre deformation gradients. These two aspects will be inserted in the FEM model as described below. The case of a sensor node modelled as a rigid body is considered first.

The high-end FEM solvers allow the user to specify constant concentrated loads, by defining their components along the model reference axis, and also permit to define how these load are applied by specifying a function of the step time. The most common option is the linear ramp variation, from 0 to 1, the full load, but it is also possible to specifity an user-defined function. This latter aspect will be referred as "amplitude" using the terminology of the Abaqus solver [29].

With reference to figure 5, the inertial effect of the acceleration is imposed on the ridig sensor node, by applying forces and constraints to the reference point. Three forces are defined into the FEM graphical interface, radial, tangential, lateral, with the components set equal to the lumped mass of the sensor. The function is set to an user-defined amplitude that returns the istantaneous acceleration to which the sensor node is subjected.

It is possible to define many different user-defined amplitudes, but these are all managed by a single routine (the `UAMP` in the case of the Abaqus solver) to which is passed the amplitude name to make possible to discriminate which component of the acceleration is to be returned. During the solver run-time, when a force is evaluated, the routine is called with the amplitude name, for discriminating the component, and the step time to perform the linear interpolation between the two nearest known values of acceleration. This value is then multiplied by the mass inserted into the component value, so defining the corresponding force magnitude $F_r(t)$ to be applied to the reference point of the sensor node.

Similarly, if the sensor node is modelled as a deformable body, it is possible to specify the components of a body-force (a force per unit volume). In this case is convenient to set the components of the body-force equal to the material density, apply the same amplitude that rescale the value by the acceleration and the result will be multiplied by each element volume and applied to it.

The accelerations measured experimentally with an accelerometer bonded to the ILare available from [3]. It is possible to save the data in an external plain text file and to load them, at the beginning of the simulation. The file is organized by Tab separated columns, with values equally spaced in time with the sampling interval Δt and it is passed to the routine as a $[t, a_r, a_t, a_l]$ matrix. The solver also passes the amplitude name to discriminate the acceleration column to be used. The step time t is also passed to the routine and it must be corrected to consider the time displacement corresponding to the angular displacement α_i:

$$t_c = t + \frac{\alpha_i}{\omega_0} \tag{8}$$

and the corresponding index to address the acceleration matrix will be: $n = \texttt{INT}(t_c/\Delta t)$. By this method it will be possible to make a linear interpolation of the acceleration value between the n and $n+1$ acceleration data.

Figure 6 shows the flow-chart of the program implemented into the `UAMP` Abaqus/Standard routine [31].

In another way the radial and tangential acceleration corresponding to the tyre deformation gradients, can be calculated in a point P at a desired vehicle speed, starting from the deformed shape given in figure 1. The point P is identified by two polar coordinates with respect to the centre of the wheel: the deformed radius, R_d, and the rotation angle, α_r. To simplify the computation it is convenient to transform the polar into cartesian coordinates:

$$\begin{Bmatrix} x \\ y \end{Bmatrix} = \begin{Bmatrix} R_d \cos(\alpha_r) \\ R_d \sin(\alpha_r) \end{Bmatrix} \tag{9}$$

Since the Cartesian coordinates of P still depend on the angular position α_r it is possible to compute the accelerations in X and Y direction deriving two times the position

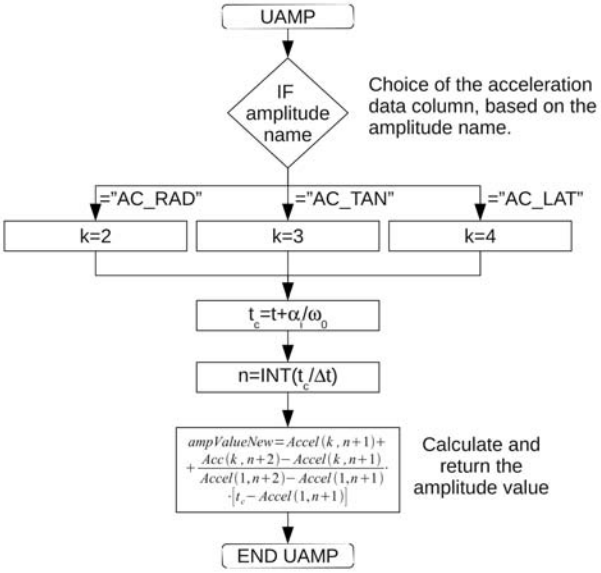

Fig. 6 Operations of the user-defined amplitude routine. Also here, the n index needs to be incremented by 1, because in `FORTRAN` the array numbering starts from 1.

whit respect to α_r and multiplying by the angular velocity squared:

$$\begin{Bmatrix} \frac{d^2x}{dt^2} \\ \frac{d^2y}{dt^2} \end{Bmatrix} = \begin{Bmatrix} \frac{d^2x}{d\alpha_r^2}\omega_0^2 \\ \frac{d^2y}{d\alpha_r^2}\omega_0^2 \end{Bmatrix} \tag{10}$$

where the derivatives can be approximated by finite differences. To have reliable results in computing derivatives it is necessary to have dense data in term of rotation angle. By way of example the numerical data in figure 7 are computed with a resolution of 0.01°, obtained by a spline interpolation of the original data at a resolution of 1°. The radial and tangential acceleration of P are computed as:

$$\begin{Bmatrix} a_r \\ a_t \end{Bmatrix} = \begin{Bmatrix} -\frac{d^2x}{dt^2}\cos(\theta) - \frac{d^2y}{dt^2}\sin(\theta) \\ -\frac{d^2x}{dt^2}\sin(\theta) + \frac{d^2y}{dt^2}\cos(\theta) \end{Bmatrix} \tag{11}$$

where θ is the angle of the tangent to the tyre in the point P, defined as:

$$\theta = 2\pi - \text{atan2}(dx, dy) \tag{12}$$

where the derivative can be again approximated by finite differences. These results are computed using a Matlab script, saved into a text file and loaded at the beginning of the simulation.

The result of the application of such technique is shown in figure 7 shows a sample of the radial and tangential acceleration acting on the sensor node derived from the deformation gradients of the tyre (continuous line), for a certain reference speed V_0 of the vehicle.

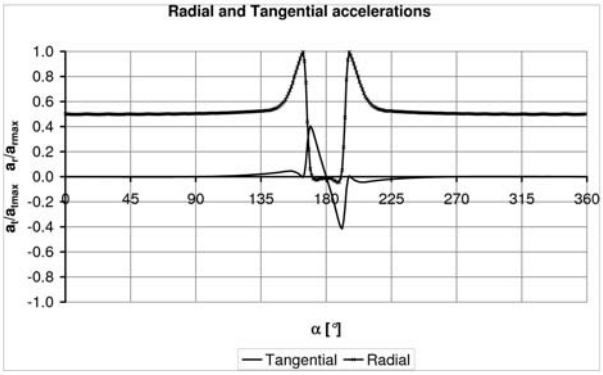

Fig. 7 Radial and tangential acceleration obtained from the deformation gradients of the tyre.

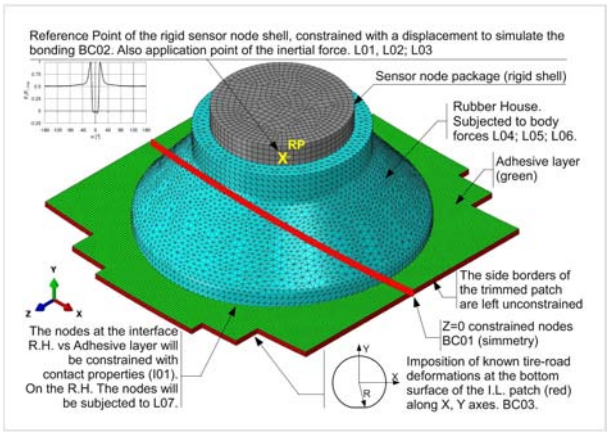

Fig. 8 FEM model. The IL patch is larger than the base of the RH as much as needed to neglect the border effects of the patch's nodes that are not constrained.

2.3 FEM Integration

Figure 8 displays the FEM model at the base of the proposed calculation method. The model of the tyre has been simplified down to a simple patch of the IL (red colour) and above it, the RH is placed and bonded on a layer of adhesive elements (green colour). Inside the RH it is encased the sensor node. The latter can be modelled as rigid shell controlled by a reference point or as deformable part, depending on its stiffness.

A typical analysis is supposed to consider a flat base RH that must be glued to the IL. In the starting condition, the base of the RH just tangent at the diametrally opposed borders of the IL.

The simulation will be carried out using the following steps:

1. RH pushing: sensor node vertical movement, to close the gap and to press its borders toward the IL; the sensor node is piloted by the reference point and it is constrained in all the other D.o.F.;

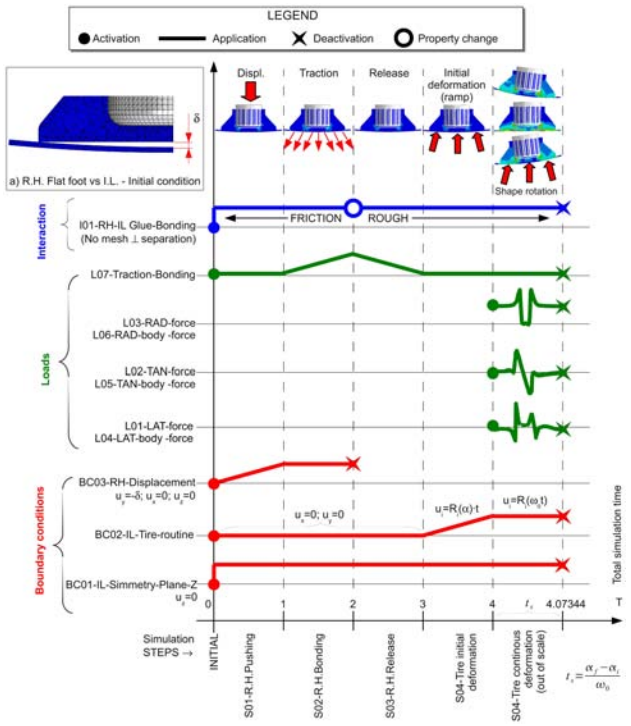

Fig. 9 Variation of the settings during the simulation.

2. RH bonding: application of a traction stress to the RH base, to make sure all the nodes of the RH close the contact with the IL nodes;
3. RH release: the contact properties change at the beginning of the step to prevent contact opening and tangential slip, in order to keep the two parts together; the traction stress is zeroed following a ramp and the other constraints of the sensor node are released;
4. Tyre initial deformation: the initial geometry of the IL (a cylinder patch) is subjected through a ramp to the deformation field at the α_i angular position;
5. Tyre continuous deformation: continuous deformation of the IL, as function of the step time applying the accelerations.

If the base were rounded, with the same radius of the internal surface of the tyre, it would be possible to tie the nodes of the RH base directly to the IL thus eliminating the first three steps.

Figure 9 displays the variation of the settings during the simulation time.

For the boundary conditions: the symmetry plane of the IL model, shown in figure 8, is constrained with a $Z = 0$ displacement for all the duration of the simulation by BC01. The remaining conditions required to fully define its position will be given by the `DISP` routine in BC02: during the first three steps, the bottom of the IL is held in place with the routine, that returns always a zero displacement. In the fourth step S04 the routine changes the form of the IL accordingly to the deformed shape in the initial angle α_i with a time ramp from 0 (undeformed) to 1 (fully deformed) using equations 3a and 3b. After that, the routine keeps the shape of the tyre and rotates it in the step time (equations 5a and 5b), until it reaches the end of the simulation time (equation 7).

The sensor node is the assembly of the sensor case (a rigid empty shell) and the RH. The external surface of the sensor node is constrained once for all to the internal cavity of the RH with a tie constraint (not shown in figure). These two assembled objects are positioned through the reference point of the sensor node using the boundary condition BC03. The subfigure 9a shows the initial gap between RH and IL δ that will be forced to close by a vertical displacement $u_2 = -\delta$ in BC03, following a time ramp, in the first step. The other positions are maintained fixed: $u_1 = u_3 = 0$. Starting from the release step the constraint is deactivated.

For the loads: in the second step, the RH has been forced to close the gap. To be sure that all the contacting nodes close the contact it is applied a slight negative pressure (about 1 Pa) with the load L07, following a time ramp. During the release step load L07 is zeroed. The RH stay glued to the IL model thanks to a change in the contact properties. On the reference point of the rigid shell are applied the three force components, radial, tangential and lateral. On the RH are applied the corresponding body force components, as sketched in figure 5. These are activated during the continuous deformation step.

The interaction properties are set from the beginning of the simulation as follows:

- normal behaviour: hard contact, with no mesh separation after the contact is closed,
- tangential behaviour: friction, with penalty formulation.

and just at the beginning of the release step the tangential behaviour is changed from friction to rough, so to avoid any tangential relative motions and effectively locking together the two parts till the end of the simulation. In the release step the sensor node is completely freed and it elastically returns, for what it is permitted by the lower surface that has a constrained contact condition.

Another point to be described is the method to import data from files external to the FEM. This is made possible by the `UEXTERNALDB` routine [31], that allows to access external data files by simply using the `OPEN`, `READ` and `CLOSE` Fortran commands [23]. Providing a plain text data file, with the values written in tab separated column the `READ` statement is able to load them directly into a vector or a matrix.

As shown in the flow-chart of figure 10, first of all `UEXTERNALDB` load a configuration file in which are declared reference radius R_0, starting and stopping angle α_i, α_f, the angular speed ω_0, the dimensions of the deformed shape vector and acceleration matrix, and the path to the files containing their saved values. The dimensions will be passed

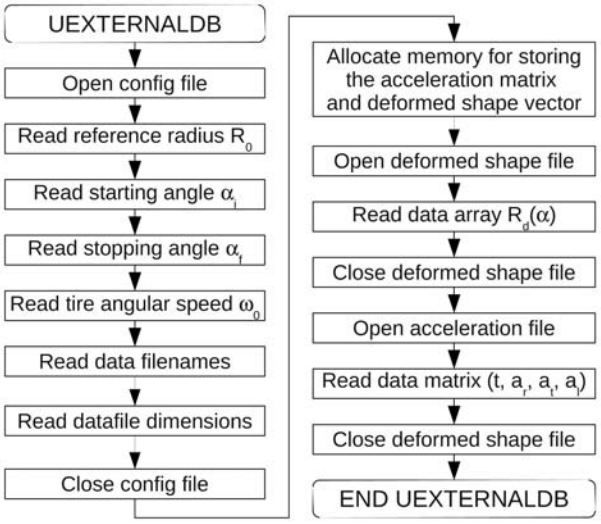

Fig. 10 `UEXTERNALDB` flowchart.

to the Fortran `ALLOCATE` command in order to reserve the RAM memory needed for storing vector and matrix; it returns a pointer to the reserved area, that is shared with all the other routines (particularly `DISP` and `UAMP`) by the `COMMON` clause. The "Configuration file" is a default file which use to allow the analyst to change quickly the simulation parameters without having to locate them into the routine file, for each new simulation.

Finally, given the limited extent of the FEM assembly, limited only to the sensor node, RH and IL, the analyst can choose the element dimensions and type in order to obtain the desired spatial resolution and H-convergence. The model being, fully constrained and with the geometrical and material non-linearity limited to few parts is stable and with an acceptable convergence rate.

Material characterization is an application specific topic, hence it will be described in the following section. The specification of temperature dependent rheological properties for the material can be avoided, as first approximation, making its tests at the temperature the tyre reaches in steady rolling.

The proposed methodology can be used in two ways. If the material mechanical characterization is available, accurate and complete (at least with an hyperelastic and viscoelastic model) it is possible to compare the simulation results with the material failure parameters and obtaining a more definite validation of the design.

If the material data are scarce, like in the examples shown here, it is possible to refine some geometrical shapes, so to reduce and make more uniform the stress concentrations. The result is an optimised geometry of the RH that must be validated by experimental tests. In this case, the application of the methodology help in reducing the number of prototype dies required for testing intermediate geometries.

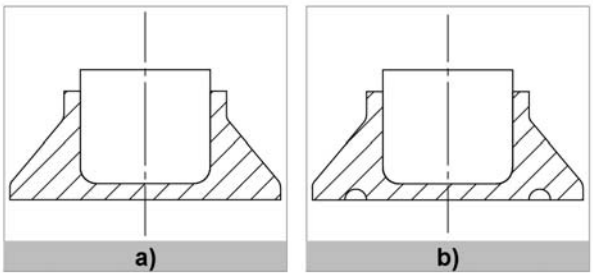

Fig. 11 Sensor node and RH CAD geometry. a) 1st attempt RH geometry b) Variation of the RH geometry for the 2nd attempt.

3 Case study

Figure 11 represents the geometry of the models used to test the present method.

The model has been set-up accordingly to the previous sections, in Abaqus/Standard [29]: the box of the sensor node has been modelled as a revolved feature and discretized using rigid elements, mixing quadrilateral (R3D4) and triangular (R3D3) shapes. The reference point for controlling the part has been set on the centre of mass position, assuming constant density. The corresponding lumped mass is equal to 10 g. The IL has been obtained as revolved part and trimmed at the borders to reduce the number of elements, obtaining the shape of figure 8. Its body has been discretized with hexaedrical elements (C3D8R) upon which a layer of cohesive elements (COH3D8) has been laid, with the aim of studying the bonding of the RH to the IL. The adhesive elements are shown in figure 8, in green colour and has been obtained by a mesh offset, equal to the glue thickness (0.01 mm), from the underlying IL surface mesh. The adhesive material response (equation 13a) has been defined in terms of traction and separation with a damage initiation criterion based on the maximum nominal stress (equation 13b) in the normal direction or in the shear direction.

$$\mathbf{t} = \begin{Bmatrix} t_n \\ t_s \\ t_t \end{Bmatrix} = \begin{bmatrix} K_{nn} & K_{ns} & K_{nt} \\ K_{ns} & K_{ss} & K_{st} \\ K_{nt} & K_{st} & K_{tt} \end{bmatrix} \begin{Bmatrix} \varepsilon_n \\ \varepsilon_s \\ \varepsilon_t \end{Bmatrix} = \mathbf{K}\boldsymbol{\varepsilon} \tag{13a}$$

$$\max \left\{ \frac{t_n}{t_n^0}, \frac{t_s}{t_s^0}, \frac{t_t}{t_t^0} \right\} = 1 \tag{13b}$$

t_n^0, t_s^0, t_t^0 represent the peak values of the nominal stress, that the material is able to bear, when the deformation is either purely normal to the interface or purely in the first or the second shear direction, respectively.

To model both the RH and the IL has been used the hyperelastic model of Yeoh and a viscoelastic model described with Prony series, in terms of relaxation modulus and relaxation time. Given the high deformation gradients of the model the corresponding stresses are not negligible.

The properties are from [13], considering the material similar to the one used in the IL.

Finally, the RH has been obtained as a revolved feature, resulting with a planar base in order to simplify the die manufacturing, and this require the bonding steps of the simulations. This kind of part has usually a complex geometry, so it has been discretized using tetrahedral elements (C3D4).

First order elements were used to simplify the solution but the same procedures can be applied to second order elements. Loads, boundary conditions and interactions have been set-up accordingly to the procedure described in 2.3.

The tyre deformed shape considered is the one obtained by a contact with the road flat surface, with a discretization of 1°. The simulation started at $\alpha_i = 30°$ and finished at $\alpha_f = 150°$ with initial and maximum time increments set corresponding to 1° in the continuous deformation step. The reference speed of the vehicle is 100 km/h and the reference radius of the IL is 320 mm. The input data used for the analyses come from Pirelli Tyre S.p.A.: the tyre deformed shape represented figure 1 is from a 3D FEM model of the tyre; the accelerometric data correspond to figure 7.

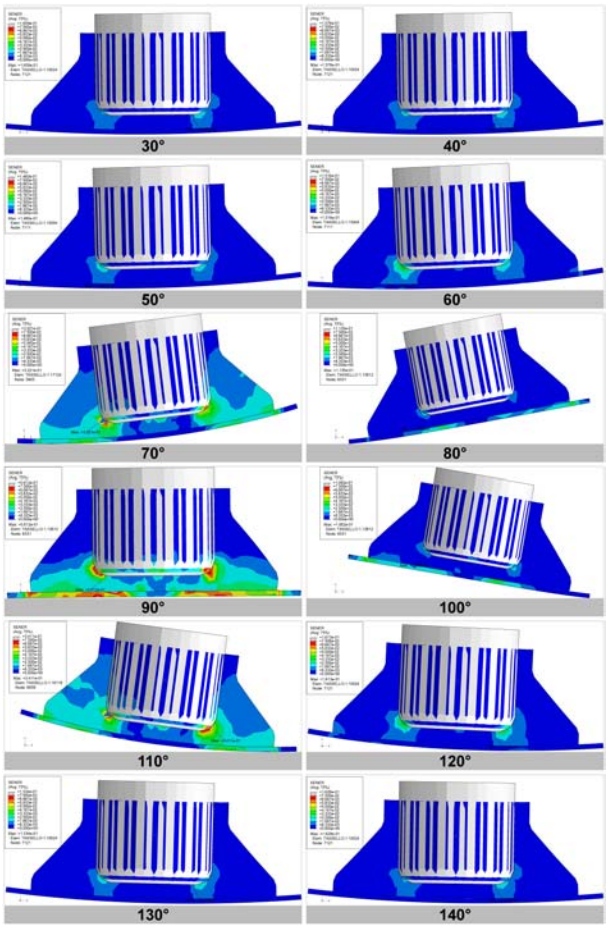

Fig. 12 Elastic strain energy density results at different step frames. The scale for the SENER field output is set for all the images between 0 and 0.075 J/cm^3. The simulation frames have been saved with an increment in the angle α of 1°, from $\alpha_i = 30°$ to $\alpha_f = 150°$. Here are reproduced the frames with a step of 10°.

3.1 Results of the 1st attempt geometry

In the result database are contained all the stress distribution for each angular position, as shown in figure 12, where some of them are represented. The first problem is to find in this amount of data the maximum stress condition: this has been done by developing a Python script run in the Abaqus/CAE graphical interface, that access and analyse the output database file (its data structure is given in [30]). For each simulation frame of the continuous deformation, the script search the maximum values of a variable specified by the user (SENER in this example) and returns a list in a plain text file with two columns: [Frame number, Max variable value] and in the last line the number of the frame in which the absolute maximum value is found. This frame will be considered for the design.

Once identified the frame, it is possible to descrive the situation as in figure 13. In this example the most stressed situation occur at the 90° position corresponding to the maximum elongation of the rubber house due to the passing through the contact area. The results that can be derived from the field output variables of the FEM solver are here listed using the naming proper to Abaqus:

- CPRESS and CSHEAR: normal and (two) tangential contact stresses, to describe the stress status at the bonding interface;
- MAXSCRT: the value of the left member parameters of equation 13b, to describe the failure status of the adhesive layer (< 1 no damage);
- SENER: element elastic strain energy, to describe with an unique quantity the stress status of the RH;
- Tresca: Tresca equivalent stress, to describe the RH material status.

Figures 13a, b, c, d, show the values of the normal contact pressure (CPRESS), the tangential stresses (CSHEAR1, CSHEAR2) at the adhesive layer interface and the damage criterion values (MAXSCRT). The values of the MAXSCRT are much lower than the limit value, so no failure is expected by the bonding of the RH and the tyre.

Figure 13e represents the elastic energy (SENER) distribution inside the material. It highlights a concentration of elastic energy around the fillet of the sensor node bottom surface, while figure 13f shows a concentration of the Tresca stress at the bottom surface of the RH near the borders of the bonded surface. These are due to the tyre stretching on the footprint plane.

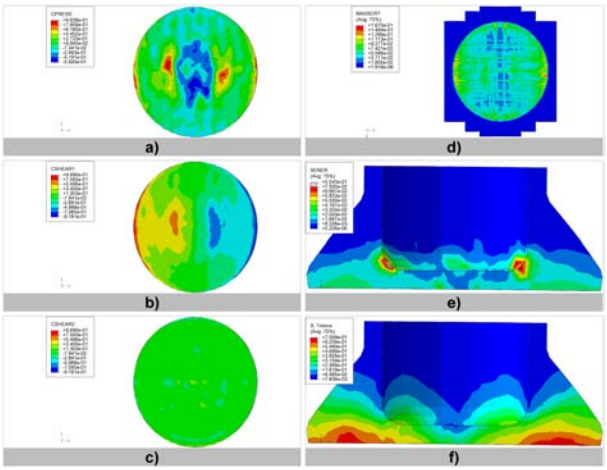

Fig. 13 Field output variables of the simulation. Bottom view of the RH. a) `CPRESS`: the normal contact pressure between RH and IL; b) `CSHEAR1`: the 1st tangential contact pressure, along the tangential stretching direction of the tyre; c) `CSHEAR2`: the 2nd tangential contact pressure, along the lateral direction. Top view of the IL. d) `MAXSCRT`: the value of the maximum tension damage criterion for the cohesive layer (1st member of eqn. 13b). Main section passing through the symmetry plane. e) `SENER` elastic strain energy density per unit volume; `Tresca`: Tresca equivalent stress. For `CSHEAR1` and `CSHEAR2` the same scale has been used. a,b,c) represent the base surface of the RH d) represents the internal surface of the IL where the cohesive layer is laid. e,f) lateral section of the RH with the IL and sensor node hidden. Main section passing through the symmetry plane.

With the aim of reducing these stress concentrations the geometry has been modified and analysed in a second simulation.

3.2 Results of the 2nd attempt geometry

Figure 11d shows the geometry considered in the second simulation: a ring-shaped groove has been added at the base of the RH. Figure 14 reproduces the comparison between the two geometrical solutions: comparing the figures 14a, b it is evident the reduction of elastic energy near the fillet of the sensor node, and in figure 14c, d it is evident the reduction of the Tresca stress.

The process can be repeated more times, until it is reached a condition for which modifying the geometry does not affect significantly the stress state of the components. The last refined geometry, can be built as prototype and tested.

Finally, some indication regarding the simulation time: the total number of elements in the first test case geometry was 81725 (all types) and the simulation ran on a workstation with a four cores Intel Xeon CPUW3530 at 2.80-GHz and 12 GB of RAM. The total CPU time for solving the problem was equal to 10 h4 min, but being the job split on four processors the real "wallclock" time was about 2-h55 min, during which the solver made a total of 141 increments, with a total of 495 equilibrium iteration, to reach the

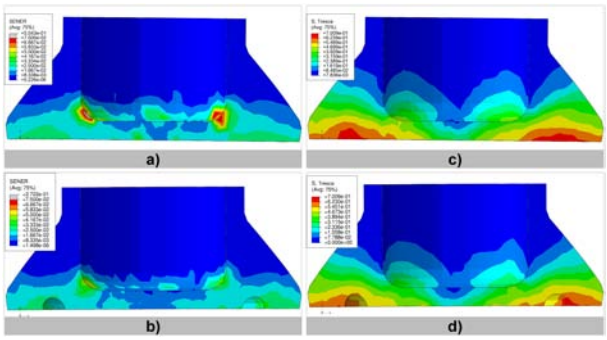

Fig. 14 Comparison of the first attempt (a, c) and second attempt geometry (b, d) of the RH. a, b) Elastic strain energy density `SENER`. c, d) `Tresca` equivalent stress.

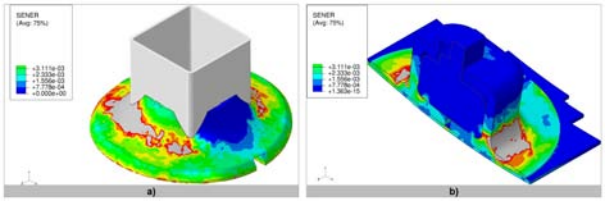

Fig. 15 Simulation results of the final products and prototypes designed with the proposed methodology. a) Pirelli Cyber™ Tyre rubber house prototype [25]. b) Pirelli Cyber™ Fleet rubber house for TPMS [26].

solution. Hence, the simulation is not too much time consuming and can be run easily on a normal desktop computer. Moreover, only two cutbacks occurred in the time incrementation, during the bonding step, confirming that the proposed methodology is stable.

3.3 Other applications

The proposed methodology has been developed during the Pirelli Cyber™ Tyre project and applied to the design of many rubber houses prototypes.

The figure 15a reproduce the simulation results of the RH prototype designed to contain the Cyber™ Tyre latest interactive sensor node under development [25], powered by an energy scavenger.

Figure 15b reproduce another kind of RH designed for floating TPMS sensors [26]. This time, the sensor node is not bonded directly to the RH internal walls, but it has a clearance of some tenth of millimiter. It can be analized with the same methodology with limited modification required: an additional contact control must be inserted between the external surface of the node package and the internal cavity of the RH, to prevent penetration, with normal contact property defined as hard contact, with the mesh free to separate if needed and the tangential behaviour set to friction penalty. The sensor node must be placed with the bottom surface tangent to the internal surfaces of the RH with the

vertical displacement set to its reference point. The following application of the traction will ensure the perfect closing of the contact between the RH base and the IL patch. During the simulation, the radial acceleration applied as body-force to the RH will deform its upper portion forcing it to contact the package. This prevents the occurrence of the situation in which the package is completely free and subjected to the inertial forces, which would cause instability in the static simulation. The product has been tested, validated and it is already on the market.

4 Conclusions

The methodology here proposed improves the design method of the RH that held fixed in position the sensor nodes glued directly to the IL of the tyre, with the aim of strengthen the road safety providing a reliable support for the sensors. This can eliminate the search of an optimum geometry by trial and testing on physical prototypes.

Into a simple static FEM simulation is possible to reproduce the most significant physical aspect of the rolling: the tyre deformed shape can be imposed by means of an user defined routine and rotated about the wheel axis, so that the RH is subjected to all the possible geometrical conditions. The inertial loads can be imposed as external forces (or body forces) modulated through an user defined amplitude. Each force component is set to the lumped mass value (or density) and the modulating amplitude returns the acceleration to which the node is subjected.

The approach is thought modular: deformed shape data, accelerometric data, solution specific parameters are saved in plain text file, and they can be changed in each new analysis to simulate different test conditions as needed. The data can be real measures obtained by mean of accelerometric sensors or can directly be derived from the deformed shape.

The tyre model can be limited only to tyre patch, for an angle reasonably bigger than the base dimension of the sensor node, so that the side border effects can be neglected. This allows to reduce the number of elements in the model and the corresponding solution time.

If the material characterization is very detailed it is possible to verify directly the mechanical resistance of the RH, if not, the results allow the comparison of different shapes and the choice of the less stressed one as candidate geometry to be tested experimentally.

The methodology has been applied to RH developed in the Pirelli Cyber™ Tyre project, with glued and floating sensor node: many geometries were analysed with the aim of reducing and smoothing the stresses inside the material, and only the last refined geometry has been produced as prototype and passed the experimental tests. This reduced significantly the investments for prototyping moulds.

5 Acknowledgements

This work has been performed under the research project "Cyber™ Tyre" funded by Pirelli Tyre S.p.A. The authors would like to thank Dr. Giorgio Audisio, Dr. Federico Mancosu, and Dr. Massimo Brusarosco from Pirelli Tyre S.p.A. for their enthusiasm and driving force in the project.

References

1. Audisio, G.: The birth of the Cyber™ Tyre. IEEE Solid-state circuits magazine **119**(2), 16 – 21 (2010). DOI 10.1109/MSSC.2010.938647
2. Bertrand, D.: Patch for fixing an electronic system to a tire. Patent (2010). US 7770444 B200
3. Bonisoli, E., Canova, A., Freschi, F., Moos, S., Repetto, M., Tornincasa, S.: Dynamic simulation of an electromechanical energy scavenging device. IEEE Transactions on Magnetics **46**(8), 2856–2859 (2010)
4. Bonisoli, E., Moos, S., Repetto, M., Tornincasa, S., Freschi, F., Mancosu, F., Brusarosco, M.: Method and system for generating electric energy in a tyre. Patent (2012). US 20120211997 A1
5. Chee, Y.H., Koplow, M., Mark, M., Pletcher, N., Seeman, M., Burghardt, F., Steingart, D., Rabaey, J., Wright, P., Sanders, S.: Picocube: A 1cm3 sensor node powered by harvested energy. In: Design Automation Conference, 2008. DAC 2008. 45th ACM/IEEE, pp. 114–119 (2008)
6. Erdogan, G., Alexander, L., Rajamani, R.: A novel wireless piezoelectric tire sensor for the estimation of slip angle. Meas. Sci. Technol. **21**(1), 015,201 (2010). DOI doi=10.1007/s00170-011-3729-0,. URL http://stacks.iop.org/0957-0233/21/i=1/a=015201
7. Erdogan, G., Alexander, L., Rajamani, R.: Estimation of tire-road friction coefficient using a novel wireless piezoelectric tire sensor. Sensors Journal, IEEE **11**(2), 267–279 (2011). DOI 10.1109/JSEN.2010.2053198
8. Ergen, S., Sangiovanni-Vincentelli, A., Sun, X., Tebano, R., Alalusi, S., Audisio, G., Sabatini, M.: The tire as an intelligent sensor. Computer-Aided Design of Integrated Circuits and Systems, IEEE Transactions on **28**(7), 941–955 (2009). DOI 10.1109/TCAD.2009.2022879
9. Fervers, C.: Improved fem simulation model for tire–soil interaction. Journal of Terramechanics **41**(2-3), 87–100 (2004). DOI 10.1016/j.jterra.2004.02.012
10. Flatscher, M., Dielacher, M., Herndl, T., Lentsch, T., Matischek, R., Prainsack, J., Pribyl, W., Theuss, H., Weber, W.: A robust wireless sensor node for in-tire-pressure monitoring. In: Solid-State Circuits Conference - Digest of Technical Papers, 2009. ISSCC 2009. IEEE International, pp. 286–287,287a (2009). DOI 10.1109/ISSCC.2009.4977420
11. Ghoreishy, M.: Finite element analysis of steady rolling tyre with slip angle: Effect of belt angle. Plastics, rubber and composites **35**(2), 83–90 (2006)
12. Ghoreishy, M.H.R.: A state of the art review of the finite element modelling of rolling tyres. Iranian Polymer Journal **17**(8), 571 – 597 (2008)
13. Ghosh, P., Saha, A., Bohara, P., Mukhopadhyay, R.: Material property characterization for finite element analysis of tires. Rubber world **233**(4), 22 – 26 (2006)
14. Global Industry Analysts, I.: Global Tire Shipments to Reach 1.7 Billion Units by 2015. (2013). URL http://www.prweb.com/releases/tires_OEM/replacement_tire/prweb4545704.htm. Accessed: May 31th, 2013

15. Hironaka, T.: Mounting structure of electronic device, and pneumatic tire onto which electronic device is mounted by such mounting structure. Patent (2009). US 2009/0266153 A1
16. Koch, R.W., Walenga, G.J., Wilson, P.B.: Method for bonding an active tag to a patch and a tire. Patent (2002). US 6444069 B1
17. Löhndorf, M., Kvisterøy, T., Westby, E., Halvorsen, E.: Evaluation of energy harvesting concepts for tire pressure monitoring systems. In: Proceedings of PowerMEMS2007 (Freiburg, Germany), pp. 331 – 334 (2007)
18. Martin, T.: Device for mounting electronic monitoring components to a tire. Patent (2007). US 7275427 B1
19. Matsuzaki, R., Todoroki, A.: Wireless strain monitoring of tires using electrical capacitance changes with an oscillating circuit. Sensors and Actuators A **119**(2), 323 – 331 (2005). DOI 10.1016/j.sna.2004.10.014
20. Matsuzaki, R., Todoroki, A.: Wireless flexible capacitive sensor based on ultra-flexible epoxy resin for strain measurement of automobile tires. Sensors and Actuators A **140**(1), 32 – 42 (2007). DOI 0.1016/j.sna.2007.06.014
21. NHTSA: Notices and final rules - TREAD Act (2001). URL http://www.nhtsa.gov/cars/rules/rulings/index_treadact.html. Accessed: May 31th, 2013
22. NHTSA: Tire pressure monitoring system FMVSS no. 138 (2001). URL http://www.nhtsa.gov/DOT/NHTSA/Rulemaking/Rules/Associated%20Files/tirepressure-fmvss-138.pdf. Accessed: May 31th, 2013
23. Nyhoff, L., Leestma, S. (eds.): Fortran 90 for engineers and scientists. Upper Saddle River: Prentice-Hall (1997)
24. Official journal of the European Union: Regulation (EC) No 661/2009 of the European Parliament and of the Council (2009). URL http://eur-lex.europa.eu/LexUriServ/LexUriServ.do?uri=OJ:L:2009:200:0001:0024:EN:PDF. Accessed: May 31th, 2013
25. Pirelli & C. S.p.A.: The pirelli Cyber™ Tyre: technical specifications (2010). URL http://www.pirelli.com/tyre/ww/en/news/2010/03/02/the-pirelli-cyber-tyre-technical-specifications. Accessed: September 17th, 2013
26. Pirelli & C. S.p.A.: Pirelli presenta Cyber™ Fleet anche in brasile (2012). URL http://www.pirelli.com/tyre/it/it/news/2012/12/05/pirelli-presenta-cybertm-fleet-anche-in-brasile/. Accessed: September 17th, 2013
27. Roundy, S., Leland, E., Baker, J., Carleton, E., Reilly, E., Lai, E., Otis, B., Rabaey, J., Wright, P., Sundararajan, V.: Improving power output for vibration-based energy scavengers. Pervasive Computing, IEEE **4**(1), 28–36 (2005). DOI 10.1109/MPRV.2005.14
28. Roundy, S., Wright, P.K., Rabaey, J.M. (eds.): Energy Scavenging for Wireless Sensor Networks. Kluwer Academic Publishers (2003). URL ISBN: 978-1-4613-5100-9
29. Simulia: Abaqus documentation - abaqus analysis user's manual (2013). URL http://www.3ds.com/products/simulia/support/documentation. Accessed: October 7th, 2013
30. Simulia: Abaqus documentation - abaqus scripting user's guide (2013). URL http://www.3ds.com/products/simulia/support/documentation. Accessed: October 7th, 2013
31. Simulia: Abaqus documentation - abaqus user subroutines reference manual (2013). URL http://www.3ds.com/products/simulia/support/documentation. Accessed: October 7th, 2013
32. Yanjin, G., Guoqun, Z., Gang, C.: 3-dimensional non-linear fem modeling and analysis of steady-rolling of radial tires. Journal of Reinforced Plastics and Composites **30**(3), 229–240 (2011)